Research Square

Preprints are preliminary reports that have not undergone peer review.
They should not be considered conclusive, used to inform clinical practice,
or referenced by the media as validated information.

Non-contrast CT radiology-clinical machine learning modeling to predict chronic hydrocephalus after aneurysmal subarachnoid hemorrhage

Haiyun Yu^
Gannan Medical University
Muyun Luo
Gannan Medical University
Hanlong Guo
Gannan Medical University
Zecun Huang
Gannan Medical University
Qiuxiang Xiao
xqx1812@163.com

Gannan Medical University

Research Article

Keywords: Radiomics, Machine learning, Aneurysmal subretinal hemorrhage, Chronic hydrocephalus

Posted Date: March 15th, 2026

DOI: https://doi.org/10.21203/rs.3.rs-8533042/v1

License: This work is licensed under a Creative Commons Attribution 4.0 International License.
Read Full License

Additional Declarations: No competing interests reported.

Abstract

Objective

To establish a machine learning model based on radiomics of non-contrast CT and clinical features to predict the occurrence of chronic hydrocephalus after aneurysmal subarachnoid hemorrhage.

Methods

A retrospective analysis of 150 patients with aneurysmal subarachnoid hemorrhage (aSAH) who underwent surgery between January 2020 and February 2024 was performed. Chronic hydrocephalus(CHC), defined as hydrocephalus occurring 14 days after ruptured aneurysmal hemorrhage, was determined primarily from follow-up CT images. Radiological features were extracted from non-contrast CT (NCCT) and screened using the least absolute shrinkage and selection algorithm (LASSO) regression method. The logistic regression (LR) model was employed to construct models by leveraging radiomic as well as clinical characteristics. A radiological-clinical nomogram model was developed and the predictive performance of the model was assessed using area under the curve (AUC), accuracy, sensitivity and specificity.

Results

A total of 150 patients were enrolled in this study. From non-contrast CT scans, 1,834 radiomic features were extracted, with 12 optimal features selected to construct the radiomic model. Univariate and stepwise multivariate analyses identified the Glasgow Coma Scale (GCS) score at admission and posterior circulation aneurysms as independent factors for constructing the clinical model. The radiomic-clinical nomogram model demonstrated area under the curve (AUC) values of 0.860 (95% CI: 0.7906–0.9303) in the training cohort and 0.683 (95% CI: 0.4795–0.8856) in the testing cohort.

Conclusion

The radiology - clinical nomogram model based on non - contrast CT shows a rather good performance in predicting chronic hydrocephalus following aneurysmal subarachnoid hemorrhage.

Introduction

Stroke, a devastating acute cerebrovascular disease, poses a serious threat to global health due to its high incidence, mortality, and disability rates. Subarachnoid hemorrhage (SAH), the third most common stroke subtype, constitutes 5% of all strokes, with a mortality rate of 25% and a disability rate of 66%[1, 2]. The etiology of SAH is multifactorial, primarily including aneurysmal rupture, vascular malformation rupture, and moyamoya disease. Among these, aneurysmal rupture is the predominant cause, typically

occurring at major arterial bifurcations of the circle of Willis. Under sustained hemodynamic stress, congenital defects in the vascular media or degenerative changes in the internal elastic lamina lead to progressive thinning and eventual rupture of the aneurysm wall [3].

The current main treatments are craniotomy clipping and endovascular coiling [4]. Despite effective interventions, many patients suffer from post-hemorrhagic complications, particularly hydrocephalus. Based on temporal onset and progression, post-aSAH hydrocephalus is classified into three categories: acute (within 72 hours), subacute (4–14 days), and chronic (> 14 days)[5, 6]. Extensive clinical studies confirm that chronic hydrocephalus is a leading cause of post-discharge readmission in aSAH patients [7], severely hindering rehabilitation, diminishing quality of life, and increasing socioeconomic burdens. Thus, rigorous post-discharge surveillance is critical for early detection and intervention. However, current clinical practice lacks reliable tools to predict chronic hydrocephalus progression.

Recent advances in big data analytics and precision medicine have highlighted the predictive power of artificial intelligence (AI) and machine learning (ML) in prognostic assessment, disease staging, and risk stratification[8–10]. Conventional imaging diagnosis heavily relies on radiologists' expertise, which may be limited in complex cases. In contrast, ML algorithms enable deep learning of high-dimensional radiomic features from medical imaging data. For instance, ML models have been successfully applied to predict futile recanalization after endovascular therapy for acute anterior circulation ischemic stroke[11]. The integration of radiomics and ML offers a promising paradigm for prognostic management by extracting latent imaging biomarkers to predict disease trajectories, therapeutic responses, and rehabilitation outcomes, thereby supporting personalized clinical decision-making.

Non-contrast CT, widely used for SAH diagnosis due to its accessibility [12], serves as the cornerstone of this study. We aim to develop an ML-based predictive model combining NCCT-derived radiomic features with clinical parameters to accurately stratify the risk of chronic hydrocephalus following aSAH. This model may enhance clinicians' ability to optimize therapeutic strategies, improve patient prognoses, and ultimately elevate long-term survival and quality of life.

Materials and methods

Patients and data acquisition

This study was approved by the Institutional Review Board (Approval No. LLSC-2025-070) with a waiver of informed consent as it involved retrospective analysis of anonymized clinical data.

Retrospective data collection of 150 patients with aneurysmal subarachnoid hemorrhage who underwent surgical treatment at our institution. The inclusion criteria were as follows: 1. age > 18 years old;2. diagnosed as aneurysmal subarachnoid hemorrhage by CTA, MRA or DSA examination in our hospital and underwent surgical treatment in our hospital. Exclusion criteria included 1. incomplete data ;2. severe artefacts or minimal bleeding on CT images ;3. loss to follow-up or postoperative follow-up <

14 days; 4. poor prognosis abandonment of treatment or death. Patients meeting the criteria were randomly divided into an 8:2 training set (n = 120) and a test set (n = 30) (Fig. 1). Chronic hydrocephalus was defined as an EVANS index > 0.3 after 14 days after onset of disease. Clinical data of these patients were obtained including age, sex, history of smoking and alcohol, hypertension, diabetes, coronary artery disease, location of aneurysm, presence of intraventricular blood, mode of surgery, presence of lumbar puncture, GCS score, Hunt-Hess score and fisher score, which were two of the authors extracted, and then another for confirmation. All patients who underwent NCCT of the head were examined using a GE Discovery CT (GE Medical, Piscataway, NJ, USA) or a Somatom Definition Flash CT (Siemens Medical Solutions, Germany). Scans were performed from the top of the head to the base of the skull with the following parameters: tube voltage 120 kV, tube current 250 mA, layer thickness 5 mm, layer spacing 5 mm. NCCT images of all patients were saved in DICOM format.

Image preprocessing and lesion segmentation

To minimize analytical errors, all non-contrast CT images underwent resampling and standardization preprocessing. Hemorrhage segmentation was performed with regions of interest (ROIs) manually delineated by a board-certified neurosurgeon with over 10 years of neurosurgical experience. To reduce subjective bias, a subset of 30 randomly selected cases were re-contoured by the same operator one month later, followed by intraclass correlation coefficient (ICC) analysis to assess feature reproducibility. Only features with ICC ≥ 0.75 were retained for subsequent modeling. ROI delineation protocol adhered to the following principles: 1. Layer-by-layer annotation of hemorrhage regions following original image slice order; 2. Precise boundary definition strictly confined to hemorrhage extent; 3. Exclusion of partial volume effects at lesion margins. The comprehensive workflow is illustrated in Fig. 2.

Radiomics feature extraction and selection

Traditional radiomic feature extraction was performed using the Pyradiomics toolkit. The derived features were categorized into three classes:

First-order features: Quantifying global intensity distributions within regions of interest (ROIs) through statistical metrics (mean, standard deviation, skewness, kurtosis).

Texture features: Characterizing spatial patterns via gray-level co-occurrence matrix (GLCM) and gray-level run-length matrix (GLRLM) analyses.

Shape features: Describing geometric properties of hemorrhagic lesions.

The feature selection pipeline comprised three sequential phases:

Phase 1: Feature Stability Screening & Normalization

Retained features with intraclass correlation coefficient (ICC) > 0.75 from test-retest segmentation to ensure reproducibility. Standardized features using Z-score normalization to mitigate scale-dependent biases. Performed Mann-Whitney U test ($p \leq 0.05$) to identify statistically discriminative features.

Phase 2: Redundancy Reduction via Correlation Filtering

Computed pairwise Pearson correlation coefficients (PCC) across features.

Eliminated redundant features (PCC > 0.9) through hierarchical clustering, retaining maximally informative representatives.

Phase 3: LASSO Regularization for Sparse Representation

Implemented least absolute shrinkage and selection operator (LASSO) regression with 10-fold cross-validation. Determined optimal penalty coefficient ($\lambda = 0.0339$) by minimizing cross-validated prediction error. Selected non-zero coefficient features to construct the final radiomics signature.

This multistage pipeline ensured feature stability (ICC > 0.75), discriminative power ($p \leq 0.05$), and non-redundancy (PCC ≤ 0.9), thereby enhancing model robustness and generalizability.

Clinical model and radiomics-clinical nomogram model construction

Firstly, the clinical features with $p \leq 0.05$ were screened by statistical analysis of the baseline data, and then using the same machine learning algorithm, the construction of the clinical model was carried out. In addition, we used 5-fold cross-validation to obtain the final clinical model. To visualize the classification evaluation, logistic regression analysis was used to construct a nomogram based on radiomics features and clinically significant features.

Statistical analysis

Normally distributed data were analyzed using the independent t-test, while the Mann-Whitney U-test was used for non-normally distributed data. Categorical variables were analyzed using chi-square test. The predictive power of the models was evaluated by plotting the subjects' job characteristics (ROC) curves and calculating the area under the curve (AUC). Statistical analyses were performed using SPSS (version 21.0; IBM Corporation) and R software (version 4.3.1). p-values ≤ 0.05 were considered statistically significant.

Results

Patient characteristics

Initially, 367 patients with aneurysmal subarachnoid hemorrhage were identified and after screening, 150 patients were finally included. The patients were randomly assigned to the training and test groups.

37.5% (45/120) of the patients with chronic hydrocephalus were in the training group and 30% (9/30) in the test group. Baseline characteristics of all patients are shown in Table 1.

Table 1
Baseline characteristics of patients

Feature	Testing Cohort (n = 30, %)	Training Cohort (n = 120, %)	pvalue
Age	57.03 ± 12.82	57.08 ± 9.98	0.985
Glasgow Coma Scale	13.07 ± 3.08	12.12 ± 3.95	0.269
Gender			0.898
Male	10(33.33)	44(36.67)	
Female	20(66.67)	76(63.33)	
Hypertension			1
No	17(56.67)	66(55.00)	
Yes	13(43.33)	54(45.00)	
Diabetes			1
No	29(96.67)	117(97.50)	
Yes	1(3.33)	3(2.50)	
CHD			1
No	29(96.67)	118(98.33)	
Yes	1(3.33)	2(1.67)	
IVH			0.438
No	17(56.67)	56(46.67)	
Yes	13(43.33)	64(53.33)	
Smoking			1
No	24(80.00)	95(79.17)	
Yes	6(20.00)	25(20.83)	
Drink			1
No	24(80.00)	98(81.67)	
Yes	6(20.00)	22(18.33)	
LP			0.205
No	18(60.00)	54(45.00)	

CHD: Coronary Heart Disease; IVH: Intraventricular Hemorrhage; LP: Lumbar Puncture

Feature	Testing Cohort (n = 30, %)	Training Cohort (n = 120, %)	pvalue
Yes	12(40.00)	66(55.00)	
Surgical procedure			0.884
Neurointerventional surgery	6(20.00)	28(23.33)	
Neurosurgical craniotomy	24(80.00)	92(76.67)	
Hunt-Hess Grading Scale			0.826
	9(30.00)	30(25.00)	
	11(36.67)	37(30.83)	
	6(20.00)	27(22.50)	
	4(13.33)	25(20.83)	
	0	1(0.83)	
Modified Fisher Scale			0.692
0	1(3.33)	1(0.83)	
	7(23.33)	23(19.17)	
	12(40.00)	52(43.33)	
	9(30.00)	34(28.33)	
	1(3.33)	10(8.33)	
Posterior circulation aneurysm			0.966
No	18(60.00)	75(62.50)	
Yes	12(40.00)	45(37.50)	
CHD: Coronary Heart Disease; IVH: Intraventricular Hemorrhage; LP: Lumbar Puncture			

Radiomics feature selection and model construction

A total of 1834 features were extracted for each patient based on the ROIs in patient imaging. Following ICC and t-test analyses, 292 stable radiomics features with between-group differences were identified in the training set. Subsequently, Pearson correlation coefficients were calculated between these features, leading to the retention of 59 features. Finally, the LASSO method was applied to the training set to determine the optimal regularization weights (λ = 0.0339), leading to the selection of 12 radiomics features for model construction. The selection of the penalty coefficient (λ = 0.0339), feature screening process, coefficient trajectories across λ values, and histogram of selected feature coefficients are

detailed in Fig. 3. These features were then input into a logistic regression (LR) model for radiomics model construction. The model achieved the AUC of 0.802(95% CI:0.7243–0.8793) in the training set, with a sensitivity of 0.867 and specificity of 0.653. In the testing set, the AUC was 0.624(95% CI:0.3892–0.8595), with a sensitivity of 0.556 and specificity of 0.667 (refer to Table 2 for more details).

Table 2
Predictive performance of three models in the training cohort and test cohort

Grouping	Model	AUC(95% CI)	Accuracy	Sensitivity	Specificity
Training Set	Clinic	0.769(0.6817–0.8564)	0.708	0.422	0.88
	Rad	0.802(0.7243–0.8793)	0.733	0.867	0.653
	Combined	0.860(0.7906–0.9303)	0.808	0.667	0.893
Testing Set	Clinic	0.675(0.4743–0.8749)	0.6	0.778	0.524
	Rad	0.624(0.3892–0.8595)	0.633	0.556	0.667
	Combined	0.683(0.4795–0.8856)	0.6	0.778	0.524

Clinical model and radiomics-clinical nomogram establishment and performance

Features for the clinical model were selected based on p-values ($p \leq 0.05$) from the training set. Multivariate analysis identified admission Glasgow Coma Scale score and posterior circulation aneurysms as independent risk factors for predicting chronic hydrocephalus after aSAH ($p \leq 0.05$) (Tables 3). In the training cohort, the clinical model achieved an AUC of 0.769 (95% CI: 0.6817–0.8564), with sensitivity and specificity values of 0.422 and 0.88, respectively. By integrating the radiomics score and clinical predictors, a radiomics-clinical nomogram was constructed (Fig. 4). The AUC values for the training and testing cohorts were 0.860 (95% CI: 0.7906–0.9303) and 0.683 (95% CI: 0.4795–0.8856), respectively. The accuracy, specificity, sensitivity, and other performance metrics of the three models are detailed in Table 2. The ROC curve comparison is presented in Fig. 5.

Table 3
Univariate and multivariate analyses for chronic hydrocephalus

Feature	Univariate Analysis		Multivariate analysis	
	OR(95%)	*p* □	OR(95%)	*p* □
Diabetes	0.5(0.067–3.747)	0.571		
CHD	1(0.098–10.237)	1		
Hypertension	0.588(0.37–0.935)	0.06		
Surgical procedure	0.673(0.474–0.954)	0.062		
Gender	0.745(0.626–0.894)	0.008	0.456(0.219–0.948)	0.078
IVH	0.778(0.405–1.177)	0.803		
Glasgow Coma Scale	0.954(0.931–0.978)	0.002	0.899(0.826–0.978)	0.038
Age	0.992(0.987–0.997)	0.023	1.02(0.994–1.047)	0.208
Modified Fisher Scale	0.98(0.895–1.111)	0.882		
LP	1.129(0.753–1.694)	0.898		
Hunt-Hess Grading Scale	1.042(0.914–1.147)	0.731		
Smoking	0.786(0.405–1.525)	0.549		
Drink	1.2(0.593–2.428)	0.67		
Posterior circulation aneurysm	2(1.189–3.364)	0.028	15.781(6.482–38.398)	<0.001
CHD: Coronary Heart Disease; IVH: Intraventricular Hemorrhage; LP: Lumbar Puncture				

In summary, the combined clinical-radiomics nomogram model demonstrated superior performance over standalone clinical and traditional radiomics models across both the training and testing cohorts in most scenarios.

Discussion

Aneurysmal subarachnoid hemorrhage is a major cause of hemorrhagic stroke worldwide, with persistently high mortality and disability rates[13–15]. Although some patients survive the acute phase, they remain at risk of severe complications such as delayed cerebral ischemia (DCI) and chronic hydrocephalus [16, 17]. In our study cohort, chronic hydrocephalus occurred in 54 of 150 patients (36%), establishing it as a prevalent sequela of aSAH that significantly impairs cognitive function, motor performance, and quality of life [18]. Current clinical management primarily relies on surgical interventions, including lumbar-peritoneal shunting and ventriculoperitoneal shunting [19, 20]. Therefore, early detection and timely intervention are critical for improving patient outcomes.

The precise mechanisms underlying post-aSAH chronic hydrocephalus remain incompletely understood, but existing evidence suggests associations with cerebrospinal fluid (CSF) dynamics abnormalities, obstruction of arachnoid granulations by blood products, and ventricular system adhesions [21]. Several risk factors have been identified, including advanced age, female sex, hypertension, higher Fisher grade on initial CT, lower initial GCS score, and higher Hunt-Hess grade at admission [22–24]. Additionally, surgical approaches significantly influence the development of chronic hydrocephalus [25, 26]. Roser et al. demonstrated that CSF output volume is an independent risk factor for shunt-dependent hydrocephalus [27]; however, due to the retrospective design of this study, complete data on this parameter were unavailable and thus excluded from analysis.

In this study, univariate and multivariate analyses identified low GCS score and posterior circulation aneurysms as significant independent risk factors for chronic hydrocephalus after aSAH. The GCS score, a key indicator of neurological status, reflects the severity of brain injury [28–30]. Patients with low GCS scores often exhibit larger hemorrhage volumes, elevated intracranial pressure, or more severe brain damage, which may directly or indirectly disrupt CSF dynamics and increase the risk of chronic hydrocephalus [31, 32]. Studies have linked low GCS scores to intraventricular hematoma accumulation, subarachnoid fibrosis, and impaired CSF absorption, all of which are critical contributors to chronic hydrocephalus[21]. Furthermore, severe cerebral edema and elevated intracranial pressure in these patients can compress the ventricular system, disrupting normal CSF flow and absorption. Prolonged mechanical ventilation and intensive care may further exacerbate these issues [33].

Low GCS scores are also associated with heightened inflammatory responses and fibrotic processes after aSAH. Inflammatory mediators in the subarachnoid space, such as cytokines and thrombin, can induce fibrosis of arachnoid granulations, impairing CSF absorption [34]. Elevated levels of inflammatory markers (e.g., IL-6, TNF-α) in the CSF of low GCS patients further correlate with chronic hydrocephalus development [35, 36]. Consistent with our findings, numerous studies confirm low GCS as an independent risk factor for chronic hydrocephalus [22, 32]. For instance, a study of 389 aSAH patients found that those with a GCS score of 15 had a 50% lower risk of shunt-dependent hydrocephalus compared to those with scores of 8–14 [37]. In our study, patients with GCS scores of 8–14 (n = 56) demonstrated a 37.5% incidence of chronic hydrocephalus (21/56), whereas those with GCS 15 (n = 68) showed a 27.9% incidence (19/68). This represents a 34.4% relative risk increase in the 8–14 group, consistent with Woernle's study.

Posterior circulation aneurysms, typically located at the basilar artery and its branches, often result in blood accumulation in the basal cisterns and posterior fossa. This can obstruct the fourth ventricular outlets, causing obstructive hydrocephalus, while basal cistern clots may induce arachnoid granulation fibrosis, impairing CSF absorption [38]. Posterior circulation hemorrhages are frequently associated with extensive SAH and intraventricular hemorrhage (IVH), the latter being a well-established independent risk factor for shunt-dependent hydrocephalus [39–41]. From a CSF dynamics perspective, IVH disrupts the balance of CSF production and absorption through multiple mechanisms. Anatomical obstruction by

blood clots can block key pathways such as the foramen of Monro, cerebral aqueduct, and fourth ventricular outlets, while inflammatory responses triggered by blood degradation products impair arachnoid granulation function [42]. These processes, combined with elevated intracranial pressure, create a vicious cycle that exacerbates CSF dysregulation [21]. In our study cohort of 150 patients, 57 (38%) harbored posterior circulation aneurysms, among whom 35 (61.4%) developed the primary endpoint of chronic hydrocephalus. In contrast, only 19 of 93 patients (20.4%) with aneurysms at other locations developed this complication. Statistical analysis revealed that posterior circulation aneurysms were associated with a nearly threefold higher risk of chronic hydrocephalus.

Advanced age serves as a core risk factor for chronic hydrocephalus following aneurysmal subarachnoid hemorrhage (aSAH), establishing a cascade pathological mechanism through multi-system interactions. Firstly, age-related cerebral atrophy expands the ventriculo-cisternal system, yet arachnoid granulation fibrosis and choroid plexus dysfunction result in a "low-reserve-high-demand" imbalance in cerebrospinal fluid (CSF) dynamics[43]. Secondly, vascular endothelial dysfunction prolongs the course of cerebral vasospasm, inducing white matter hypoperfusion and vasogenic edema, which further disrupt the homeostasis of the CSF-brain tissue interface. Concurrently, immunosenescence drives excessive release of pro-inflammatory cytokines (e.g., interleukin-6 [IL-6], tumor necrosis factor-α [TNF-α]), causing irreversible stenosis of CSF pathways[44]. Additionally, concomitant metabolic syndrome inhibits Na^+/K^+-ATPase activity and activates the mTOR pathway through advanced glycation end products (AGEs), forming a positive feedback loop of neuroinflammation[45]. These cross-system pathophysiological processes collectively form a high-risk network for CHC development in elderly patients, highlighting the profound impact of the overall dysfunction of the neuro-vascular-immunometabolic axis during aging on CSF circulation.

In imaging stratification, Fisher grade □-□ is strongly associated with CSF circulation disorders and inflammatory fibrosis due to massive hemorrhage, whereas Hunt-Hess grade IV–V patients exhibit significantly elevated CHC risk [22, 39, 46].Surgical approaches differentially influence outcomes: surgical clipping, with its greater invasiveness and inflammatory response, predisposes to arachnoid granulation fibrosis (a Japanese database study revealed a twofold higher CHC risk compared to coiling)[47]. In contrast, endovascular coiling, while minimizing tissue damage, may increase intraventricular hemorrhage risk due to mandatory antiplatelet therapy. Notably, a Korean cohort study stratified by Fisher grade demonstrated procedure-specific risk variations: coiling showed lower CHC incidence in low-grade subgroups, whereas clipping outperformed in high-grade cases [48]. Clinically, third ventriculostomy is frequently combined with clipping to optimize CSF circulation, effectively reducing reoperation rates[49, 50].

Recent advances in radiomics and machine learning have revolutionized precision medicine. Radiomics enables high-throughput extraction of quantitative imaging features (e.g., shape, texture, intensity) from medical images, which, when combined with clinical data (e.g., age, sex, scale scores), can build robust predictive models [51, 52]. For instance, in oncology, radiomics has been used to assess tumor

heterogeneity, microenvironment, and treatment response[53]. In aSAH, CT-based radiomics can objectively quantify intraventricular hemorrhage, SAH volume, and clot thickness, which are known predictors of chronic hydrocephalus. By integrating these imaging features with postoperative clinical data, ML models can identify high-risk patients early.

This study innovatively proposes a multimodal fusion model based on NCCT images, combining traditional radiomic features with clinical data to enhance the predictive accuracy of chronic hydrocephalus after aSAH. Results demonstrate that the fusion model outperforms single-modality approaches, likely due to the synergistic effects of multidimensional data. Radiomic features capture hemorrhage characteristics, while clinical data reflect pathophysiological states, overcoming the limitations of individual models. The combined model achieved higher AUC and accuracy in both training and testing cohorts, with decision curve analysis confirming its superior clinical utility. These findings suggest that ML models can serve as reliable tools to guide clinical decision-making.

Despite its clinical significance, this study has limitations. As a single-center retrospective analysis, it may be subject to selection bias and information bias due to the exclusion of cases with incomplete data, potentially limiting generalizability. The relatively small sample size (n = 150) and single-institution data may introduce confounding factors, such as population homogeneity and regional treatment variations, restricting external validation and clinical translation. Additionally, the retrospective design precluded the inclusion of key prognostic factors (e.g., total CSF drainage volume, fibrinolysis markers). Future multicenter prospective studies with larger, more diverse cohorts are needed to validate these findings. Incorporating advanced techniques such as deep learning for automated image analysis (e.g., ventricular volume dynamics, 3D hematoma reconstruction) and multi-omics biomarkers could further refine predictive models. Real-time CSF dynamics monitoring and infection-related inflammatory markers should also be integrated to better elucidate the multifactorial mechanisms of chronic hydrocephalus.

Conclusion

The radiology - clinical machine learning model leveraging pre - operative non - contrast computed tomography data has yielded positive results in predicting chronic hydrocephalus in patients with aneurysmal subarachnoid hemorrhage. This model holds the potential to assist neurologists in promptly assessing patients' prognostic outcomes and providing valuable insights for personalized treatment strategies.

Declarations

Acknowledgements

Thanks to the Big Data Center of Gannan Medical University for its generous support for this research.

Author contributions

Haiyun Yu: Conceptualization, Data curation, Formal analysis, Writing – original draft. Muyun Luo: Data Curation, Formal analysis, Validation. Zecun Huang: Data Curation, Validation. Hanlong Guo: Data Curation. Qiuxiang Xiao: Conceptualization, Resources, Supervision, Writing – review & editing. All the authors took part in the experiment. All the authors read and approvaled the manuscript.

Funding

This study was supported by the Guiding Technology Program of Ganzhou City (GZ2024SF156), the Ganzhou Science and Technology Bureau Project (GZ2021ZSF060 and 2023LNS37747).

Data availability

The data supporting the findings of this study are not publicly disclosed due to the involvement of patient privacy.

Ethics approval and consent to participate

This study was conducted in accordance with the relevant principles of the Declaration of Helsinki. The study protocol was approved by the Ethics Committee of the First Affiliated Hospital of Gannan Medical University (Approval No.: LLSC-2025-070). As this was a retrospective analysis with no risk of privacy disclosure, informed consent from patients was waived.

Consent for publication

Not applicable.

Competing interests

The authors declare no competing interests.

References

1. LV B, LAN J X, SI Y F, et al. Epidemiological trends of subarachnoid hemorrhage at global, regional, and national level: a trend analysis study from 1990 to 2021 [J]. Mil Med Res. 2024;11(1):46.
2. WEILAND J, BEEZ A, WESTERMAIER T et al. Neuroprotective Strategies in Aneurysmal Subarachnoid Hemorrhage (aSAH) [J]. Int J Mol Sci, 2021, 22(11).
3. CLAASSEN J, PARK S. Spontaneous subarachnoid haemorrhage [J]. Lancet. 2022;400(10355):846–62.
4. HOH B L, KO N U, AMIN-HANJANI S, et al. 2023 Guideline for the Management of Patients With Aneurysmal Subarachnoid Hemorrhage: A Guideline From the American Heart Association/American Stroke Association [J]. Stroke. 2023;54(7):e314–70.
5. KWON J H, SUNG S K, SONG Y J, et al. Predisposing factors related to shunt-dependent chronic hydrocephalus after aneurysmal subarachnoid hemorrhage [J]. J Korean Neurosurg Soc.

2008;43(4):177–81.
6. CHEN S, LUO J, REIS C et al. Hydrocephalus after Subarachnoid Hemorrhage: Pathophysiology, Diagnosis, and Treatment [J]. Biomed Res Int, 2017, 2017: 8584753.
7. GREENBERG JK, WASHINGTON C W, GUNIGANTI R, et al. Causes of 30-day readmission after aneurysmal subarachnoid hemorrhage [J]. J Neurosurg. 2016;124(3):743–9.
8. WANG X, ZHAO J. A pathology foundation model for cancer diagnosis and prognosis prediction [J]. Nature. 2024;634(8035):970–8.
9. CHEN Y, WANG B, ZHAO Y, et al. Metabolomic machine learning predictor for diagnosis and prognosis of gastric cancer [J]. Nat Commun. 2024;15(1):1657.
10. LI Y, WU X. Machine Learning for Lung Cancer Diagnosis, Treatment, and Prognosis [J]. Genomics Proteom Bioinf. 2022;20(5):850–66.
11. SUN T, YU H Y, ZHAN C H, et al. Non-contrast CT radiomics-clinical machine learning model for futile recanalization after endovascular treatment in anterior circulation acute ischemic stroke [J]. BMC Med Imaging. 2024;24(1):178.
12. WESTERLAAN H E, VAN DIJK J M, JANSEN-VAN DER WEIDE M, C, et al. Intracranial aneurysms in patients with subarachnoid hemorrhage: CT angiography as a primary examination tool for diagnosis–systematic review and meta-analysis [J]. Radiology. 2011;258(1):134–45.
13. NEIFERT S N, CHAPMAN E K, MARTINI ML, et al. Aneurysmal Subarachnoid Hemorrhage: the Last Decade [J]. Transl Stroke Res. 2021;12(3):428–46.
14. ZHANG Q, ZHANG J. MO J. Pharmacological Modulations of Nrf2 and Therapeutic Implications in Aneurysmal Subarachnoid Hemorrhage [J]. Molecules, 2023, 28(4).
15. CHAI C Z, HO U C. KUO L T. Systemic Inflammation after Aneurysmal Subarachnoid Hemorrhage [J]. Int J Mol Sci, 2023, 24(13).
16. ABDULAZIM A, HEILIG M, RINKEL G, et al. Diagnosis of Delayed Cerebral Ischemia in Patients with Aneurysmal Subarachnoid Hemorrhage and Triggers for Intervention [J]. Neurocrit Care. 2023;39(2):311–9.
17. MASSON A, BOULOUIS G, JANOT K, et al. Acute hydrocephalus and delayed cerebral infarction after aneurysmal subarachnoid hemorrhage [J]. Acta Neurochir (Wien). 2022;164(9):2401–8.
18. WESTERN E, SORTEBERG A, BRUNBORG C, et al. Prevalence and predictors of fatigue after aneurysmal subarachnoid hemorrhage [J]. Acta Neurochir (Wien). 2020;162(12):3107–16.
19. PARASRAM M, PARK J, AL-DULAIMI M, W, et al. Guidelines in Action: Management of Acute and Chronic Hydrocephalus Following Aneurysmal Subarachnoid Hemorrhage [J]. Stroke. 2023;54(12):e508–11.
20. LI X, WANG Y, XIA B, et al. Lumboperitoneal shunt and ventriculoperitoneal shunt for chronic hydrocephalus after aneurysmal subarachnoid hemorrhage: a comparison [J]. Front Surg. 2024;11:1368493.

21. KUO L T, HUANG AP. The Pathogenesis of Hydrocephalus Following Aneurysmal Subarachnoid Hemorrhage [J]. Int J Mol Sci, 2021, 22(9).
22. SANUSI T D, MCLARNON M. Risk factors of chronic shunt dependent hydrocephalus following aneurysmal subarachnoid haemorrhage [J]. Clin Neurol Neurosurg. 2020;198:106095.
23. GOLLWITZER M, STEINDL M, STROH N, et al. Machine Learning-Based Prediction of Chronic Shunt-Dependent Hydrocephalus After Spontaneous Subarachnoid Hemorrhage [J]. World Neurosurg. 2024;192:e124–33.
24. MUSCAS G, MATTEUZZI T. Development of machine learning models to prognosticate chronic shunt-dependent hydrocephalus after aneurysmal subarachnoid hemorrhage [J]. Acta Neurochir (Wien). 2020;162(12):3093–105.
25. GARVAYO M, MESSERER M. The positive impact of cisternostomy with cisternal drainage on delayed hydrocephalus after aneurysmal subarachnoid hemorrhage [J]. Acta Neurochir (Wien). 2023;165(1):187–95.
26. JIANG W. Effect of combined fenestration of lamina terminalis and Liliequist membrane during surgical clipping on the incidence of chronic hydrocephalus in patients with anterior circulation ruptured aneurysms [J]. Clin Neurol Neurosurg. 2023;224:107575.
27. GARCíA-ARMENGOL R, PUYALTO P, MISIS M, et al. Cerebrospinal Fluid Output as a Risk Factor of Chronic Hydrocephalus After Aneurysmal Subarachnoid Hemorrhage [J]. World Neurosurg. 2021;154:e572–9.
28. TEASDALE G, MAAS A, LECKY F, et al. The Glasgow Coma Scale at 40 years: standing the test of time [J]. Lancet Neurol. 2014;13(8):844–54.
29. AHMADI S, SARVEAZAD A, BABAHAJIAN A, et al. Comparison of Glasgow Coma Scale and Full Outline of UnResponsiveness score for prediction of in-hospital mortality in traumatic brain injury patients: a systematic review and meta-analysis [J]. Eur J Trauma Emerg Surg. 2023;49(4):1693–706.
30. BRENNAN PM, WHITTINGHAM C, SINHA VD, et al. Assessment of level of consciousness using Glasgow Coma Scale tools [J]. BMJ. 2024;384:e077538.
31. FANG H Y, LIN C Y, KO W J. Hematology and coagulation parameters predict outcome in Taiwanese patients with spontaneous intracerebral hemorrhage [J]. Eur J Neurol. 2005;12(3):226–32.
32. CZORLICH P, RICKLEFS F, REITZ M, et al. Impact of intraventricular hemorrhage measured by Graeb and LeRoux score on case fatality risk and chronic hydrocephalus in aneurysmal subarachnoid hemorrhage [J]. Acta Neurochir (Wien). 2015;157(3):409–15.
33. LI A, ATEM F D, VENKATACHALAM A M, et al. Admission Glasgow Coma Scale Score as a Predictor of Outcome in Patients Without Traumatic Brain Injury [J]. Am J Crit Care. 2021;30(5):350–5.
34. BRAUN M, BOSTRöM G, INGELSSON M, et al. Levels of inflammatory cytokines MCP-1, CCL4, and PD-L1 in CSF differentiate idiopathic normal pressure hydrocephalus from neurodegenerative diseases [J]. Fluids Barriers CNS. 2023;20(1):72.

35. HABIYAREMYE G, MORALES D M, MORGAN C D, et al. Chemokine and cytokine levels in the lumbar cerebrospinal fluid of preterm infants with post-hemorrhagic hydrocephalus [J]. Fluids Barriers CNS. 2017;14(1):35.
36. SHEN Y, LI C, ZHANG X, et al. Gut microbiota linked to hydrocephalus through inflammatory factors: a Mendelian randomization study [J]. Front Immunol. 2024;15:1372051.
37. WOERNLE C M, WINKLER K M BURKHARDTJK, et al. Hydrocephalus in 389 patients with aneurysm-associated subarachnoid hemorrhage [J]. J Clin Neurosci. 2013;20(6):824–6.
38. GöTTSCHE J, PIFFKO A, PANTEL T F, et al. Aneurysm Location Affects Clinical Course and Mortality in Patients With Subarachnoid Hemorrhage [J]. Front Neurol. 2022;13:846066.
39. WU B, ZHOU Y, FAN H, et al. Cerebrospinal fluid drainage and chronic hydrocephalus in aneurysmal subarachnoid hemorrhage patients with intraventricular hemorrhage [J]. Front Neurol. 2023;14:1302622.
40. GRUBER A, REINPRECHT A, BAVINZSKI G et al. Chronic shunt-dependent hydrocephalus after early surgical and early endovascular treatment of ruptured intracranial aneurysms [J]. Neurosurgery, 1999, 44(3): 503-9; discussion 9–12.
41. CATAPANO JS, RUMALLA K, KARAHALIOS K, et al. Intraventricular Tissue Plasminogen Activator and Shunt Dependency in Aneurysmal Subarachnoid Hemorrhage Patients With Cast Ventricles [J]. Neurosurgery. 2021;89(6):973–7.
42. MORIYA M, KARAKO K, MIYAZAKI S, et al. Interpretable machine learning model for outcome prediction in patients with aneurysmatic subarachnoid hemorrhage [J]. Crit Care. 2025;29(1):36.
43. LI W, LI J, LI J, et al. Boosting neuronal activity-driven mitochondrial DNA transcription improves cognition in aged mice [J]. Science. 2024;386(6728):eadp6547.
44. JIANG J, HIRON T K, AGBAEDENG T A, et al. A Novel Macrophage Subpopulation Conveys Increased Genetic Risk of Coronary Artery Disease [J]. Circ Res. 2024;135(1):6–25.
45. HUANG Z, ZHU L, CAO Y, et al. ASD: a comprehensive database of allosteric proteins and modulators [J]. Nucleic Acids Res. 2011;39(Database issue):D663–9.
46. ZHANG F, CAI X F, ZHAO W, et al. A Predictive Model for Chronic Hydrocephalus After Clipping Aneurysmal Subarachnoid Hemorrhage [J]. J Craniofac Surg. 2023;34(2):680–3.
47. YAMADA S, ISHIKAWA M, YAMAMOTO K, et al. Aneurysm location and clipping versus coiling for development of secondary normal-pressure hydrocephalus after aneurysmal subarachnoid hemorrhage: Japanese Stroke DataBank [J]. J Neurosurg. 2015;123(6):1555–61.
48. NAM K H, HAMM I S, KANG D H, et al. Risk of Shunt Dependent Hydrocephalus after Treatment of Ruptured Intracranial Aneurysms: Surgical Clipping versus Endovascular Coiling According to Fisher Grading System [J]. J Korean Neurosurg Soc. 2010;48(4):313–8.
49. ZWIMPFER T J, SALTERIO N WILLIAMSMA, et al. Cognitive and gait outcomes after primary endoscopic third ventriculostomy in adults with chronic obstructive hydrocephalus [J]. J Neurosurg. 2022;136(3):887–94.

50. KUMAR S, SAHANA D. Extra-axial endoscopic third ventriculostomy: preliminary experience with a technique to circumvent conventional endoscopic third ventriculostomy complications [J]. J Neurosurg. 2023;138(2):503–13.
51. HANDELMAN GS, KOK H K, CHANDRA RV, et al. eDoctor: machine learning and the future of medicine [J]. J Intern Med. 2018;284(6):603–19.
52. CHEN M, COPLEY S J, VIOLA P, et al. Radiomics and artificial intelligence for precision medicine in lung cancer treatment [J]. Semin Cancer Biol. 2023;93:97–113.
53. LIN C Y, GUO S M LIENJJ, et al. Combined model integrating deep learning, radiomics, and clinical data to classify lung nodules at chest CT [J]. Radiol Med. 2024;129(1):56–69.

Figures

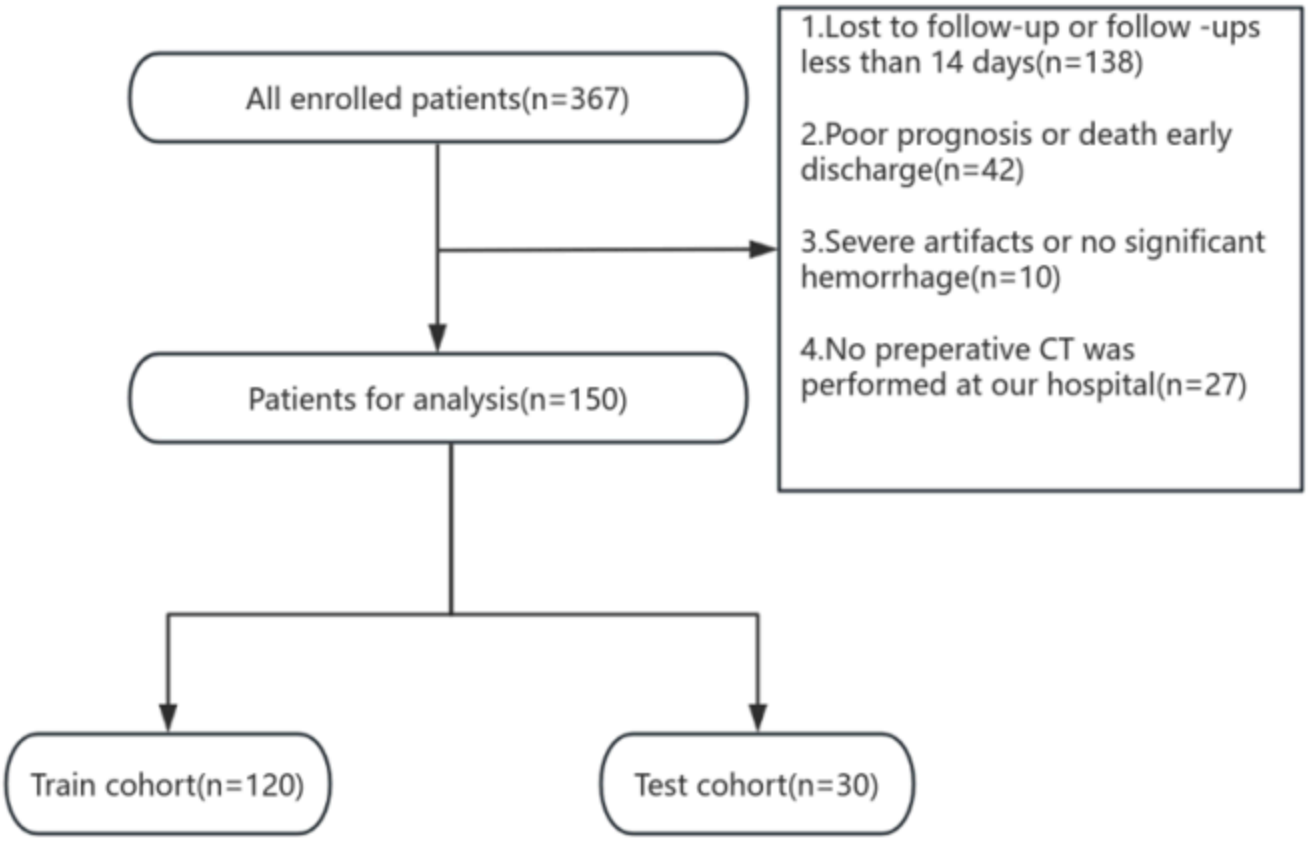


Figure 1

The flow chart for the exclusion of patients

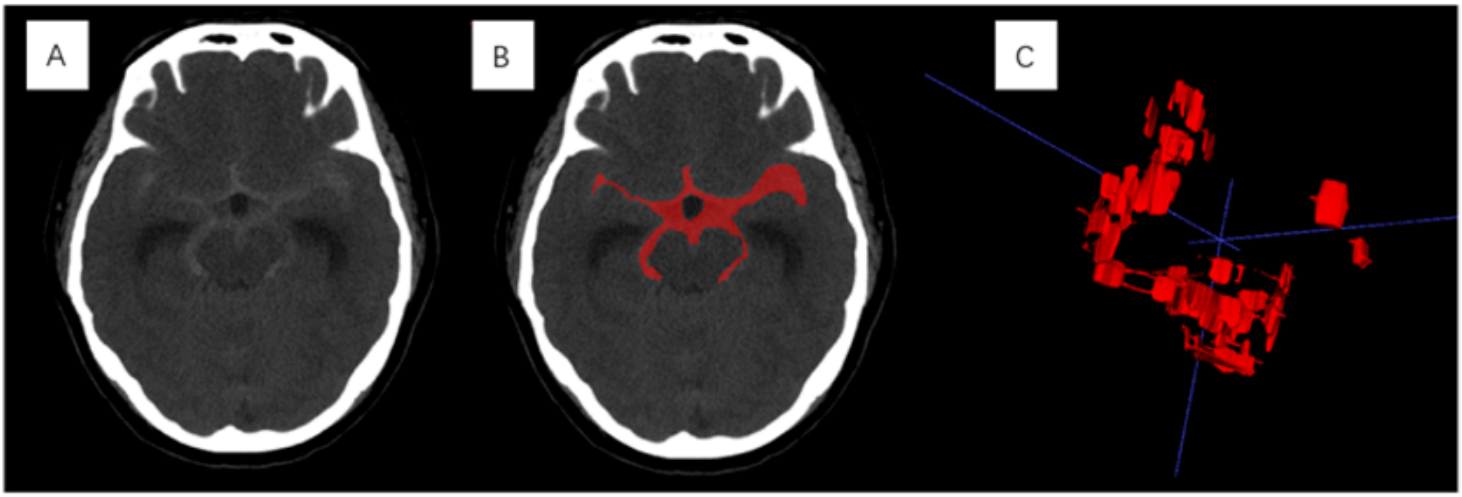


Figure 2

Schematic Diagram of Specific ROI Delineation Steps.

A. Pre-delineation image of a single patient slice; B. Post-delineation image of the same patient slice; C. ROI after delineation across all slices (3D image).

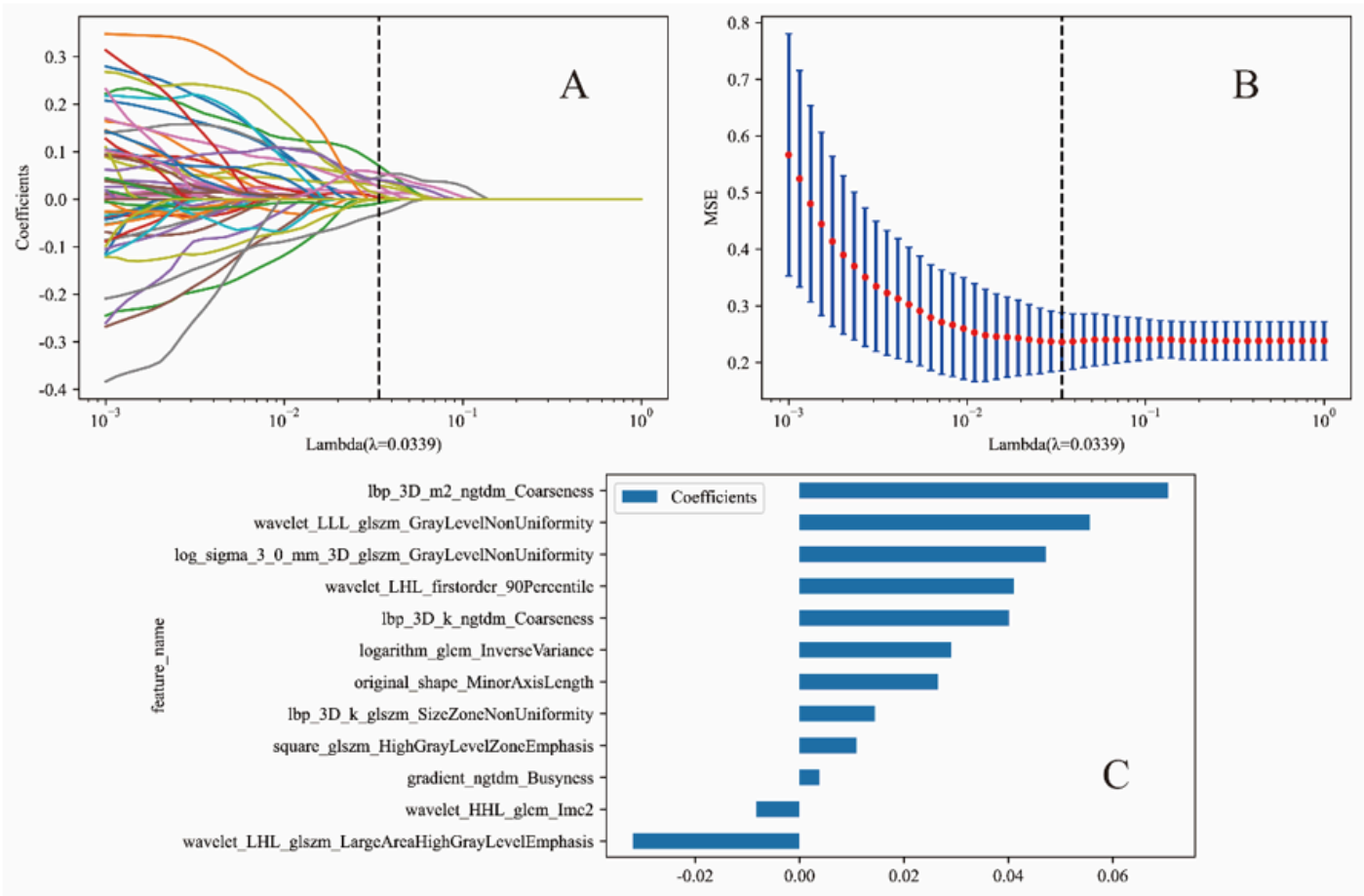


Figure 3

Radiomics Feature Selection Process Based on LASSO Regression

A. Coefficient Shrinkage Path Diagram (λ) B. Ten-Fold Cross-Validation Error Curve C. Histogram of Selected Feature Coefficient Distribution

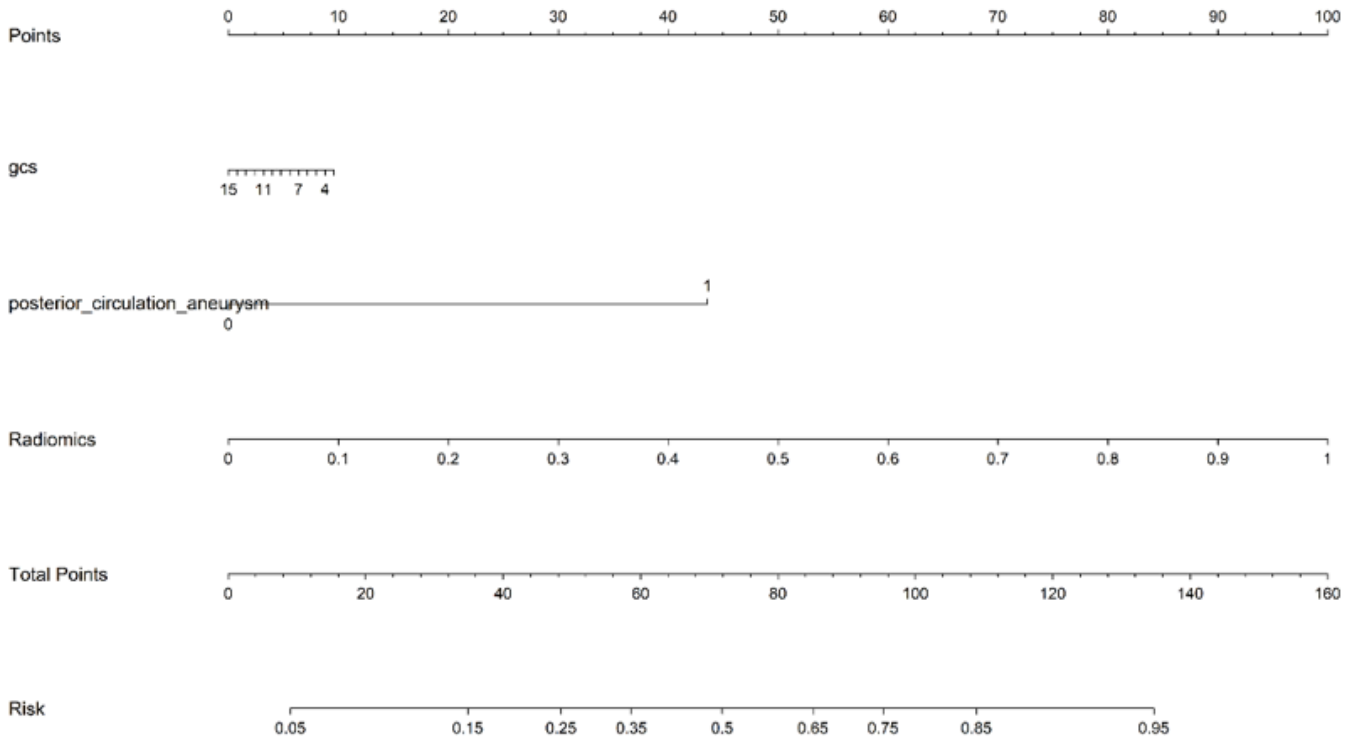


Figure 4

Radiomics Nomogram Based on Machine Learning

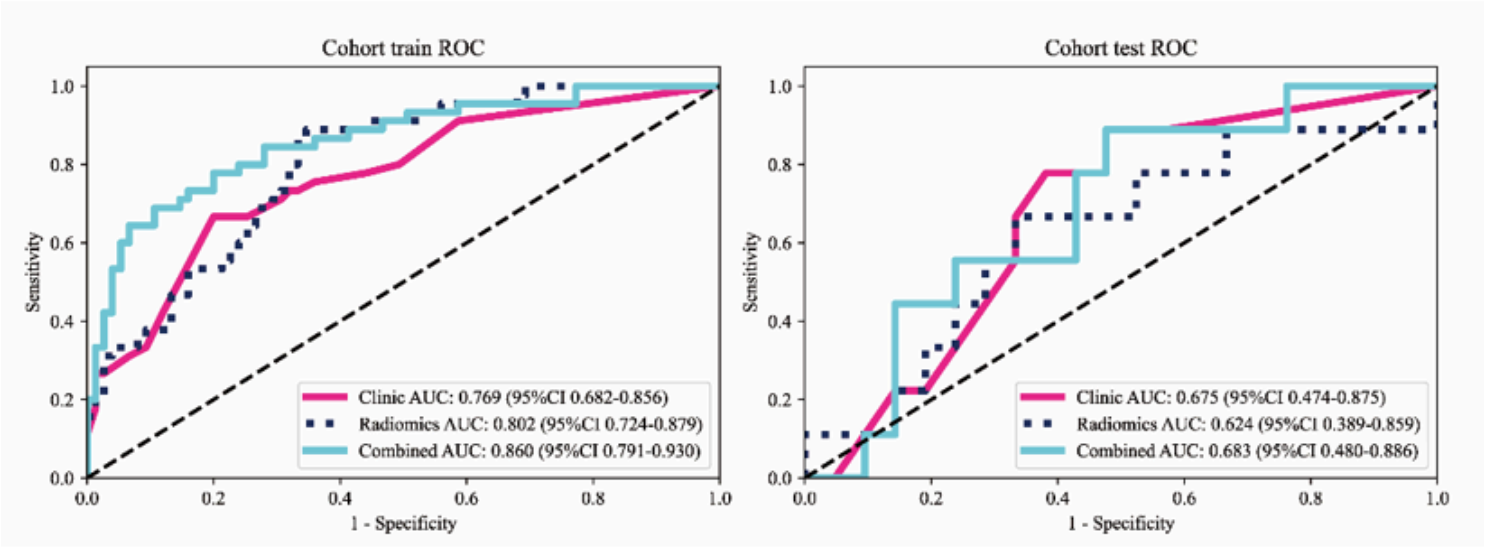


Figure 5

ROC curves of various models in the training (left) and testing sets (right)